Electronic Supplementary Material (ESI) for Energy & Environmental Science.

Supporting Information for:

Furfural Electrovalorisation Using Single-atom Molecular Catalysts

Zamaan Mukadam[1,‡], Sihang Liu[2,‡], Angus Pedersen[1,3], Jesús Barrio[1,3], Sarah Fearn[1], Saurav Ch. Sarma[3], Maria-Magdalena Titirici[3], Soren B. Scott*[1], Ifan E. L. Stephens*[1], Karen Chan[2], Stefano Mezzavilla*

Affiliations:
[1]Department of Materials, Imperial College London, London, UK.
[2]Catalysis Theory Center, Department of Physics, Technical University of Denmark (DTU), 2800 Kgs. Lyngby, Denmark.
[3]Department of Chemical Engineering, Imperial College London, London, UK.
[‡]These authors contributed equally.

Supplementary experimental methods

XPS X-ray photoelectron spectroscopy (XPS) was carried out in a Thermo Fisher K-Alpha XPS system. The spectra were analysed with the Avantage software. All spectra were calibrated relative to the carbon C1s peak at 284.8 eV for correcting for charging effects.

NMR ^{1}H Nuclear Magnetic Resonance was carried out on a Bruker AV400 spectrometer at 400 MHz. Deuterated chloroform (99.8% $CDCl_3$, Sigma Aldrich) was used as the solvent with MestReNova software being used to analyse the spectra.

High-angle Annular Dark-field Scanning Transmission Electron Microscopy (HAADF-STEM)
Scanning Transmission Electron Microscopy (STEM) was carried out for the direct imaging of single atoms in a JEOL ARM200F at 200 kV and the images analysed with the Gatan software. STEM samples were deposited onto the grids in dry condition to avoid solvent contamination.

Supplementary computational methods

Electronic adsorption energies of adsorbate *ads*, e.g., furfural (FCHO) and hydrogen (H) were calculated as follows:

$$\Delta E_{ads} = E_{ads + slab} - E_{ads(g)} - E_{slab} \quad \text{(S1)}$$

where $E_{ads + slab}$, $E_{ads(g)}$, and E_{slab} are the DFT-calculated energy of adsorbate on the surface, adsorbate in gas phase, and clean surface.

Gibbs free energies for adsorbed intermediates at 298.15 K were derived from DFT-calculated energies by using vibrations obtained from harmonic thermochemistry using IBRION = 5 with all slab atoms fixed and only adsorbates relaxed, which were calculated as:

$$G_{ads} = E_{ads} + ZPE - TS \quad \text{(S2)}$$

where E_{ads}, ZPE and S are the DFT-calculated energy, zero-point energy and entropy of the adsorbate.

As for the calculations of free energies for liquid-phase furfural and hydrofuroin, we simulated the gas-phase molecules and obtained free energy correction based on ideal gas thermochemistry embedded in ASE with a vapor pressure of ca. 150Pa at room temperature based on previous experiments.[1] The Gibbs free energies of reactants and products were then used to calculate the equilibrium potentials for reduction reactions shown in Scheme 1 based on Nernst equation.

In general, the electrochemical reduction of furfural is described by the equation:

$$xFCHO + n\left(H^{+} + e^{-}\right) \rightarrow yProduct + mH_{2}O \quad \text{(S3)}$$

$$\Delta G^{0}_{xFCHO \rightarrow yProduct} = \sum v_i(\Delta_f G^{0}_{i}) = y\Delta_f G^{0}_{product} + m\Delta_f G^{0}_{H2O} - x\Delta_f G^{0}_{FCHO} - n\Delta_f G^{0}_{\left(H^{+} + e^{-}\right)} \quad \text{(S4)}$$

The computational hydrogen electrode (CHE) postulated by Nørskov et al.[2] was used to determine the reaction free energy diagrams as a function of the applied potential versus RHE scale. The chemical potential of the proton can be related to that of H_2 at 0V versus RHE:

$$\mu_{H^{+}} + \mu_{e^{-}} = \frac{1}{2}\mu_{H_2}(g) \quad \text{(S5)}$$

Thus,

$$\Delta_f G^{0}_{\left(H^{+} + e^{-}\right)} = -FU_{RHE} \quad \text{(S6)}$$

$$U^{0} = -\left(y\Delta_f G^{0}_{product} + m\Delta_f G^{0}_{H2O} - x\Delta_f G^{0}_{FCHO}\right)/nF \quad \text{(S7)}$$

where F is the Faradays constant, n is the electron number transferred to produce one product molecule (n = 2 for FAL and Hydrofuroin, 4 for 2-MF) and $\Delta G^{0}_{xFCHO \rightarrow yProduct}$ is the Gibbs free reaction energy at standard conditions.

The spin-polarized FCHOH radical energy was estimated by the Gibbs free energy FCHOH radical simulated in vacuum using Ideal-gas limit in ASE Thermochemistry, where the spin is set as 0.5 for a single unpaired electron and the pressure is set as the same as furfural.

Supplementary tables

Table S1. Major products for furfural electroreduction on different catalysts reported in previous experiments. The selectivity map shown in Figure 1b is based on the relative selectivity values in this table.

Catalyst	Potential (V vs RHE)	Total current density (mA/cm^2)	Selectivity (%)				Furfural Concentration (M)	Electrolyte	Reference
			FAL	MF	HF	H_2			
Al	-	10	-	-	83	-	0.05	0.5 M H_2SO_4 and water–acetonitrile mixture	3
Ag	-0.5	-	65	-	-	-	0.1	0.1 M sodium phosphate buffer at pH 6.8	4
Au	-	75	35	-	-	-	0.25	1 M H_2SO_4	5
Carbon	-	10	10	-	70	-	0.05	0.5 M H_2SO_4 and water–acetonitrile mixture	3
Cu	-	10	10	80	-	-	0.05	0.5 M H_2SO_4 and water–acetonitrile mixture	3
Cu	-0.55	-	40	30	-	12	0.05	0.5 M sulfate solutions at pH 3.0	6
Cu	-0.75	-	95	-	-	3	0.04	phosphate buffer at pH 8.0	7
Ni	-	10	32	28	12	-	0.05	0.5 M H_2SO_4 and water–acetonitrile mixture	3
Ni	-0.65	10-15	80	-	-	-	0.08	0.1 M NaOH	8
Pb	-	10	20	-	60	-	0.05	0.5 M H_2SO_4 and water–acetonitrile mixture	3
Pd	-0.5	-	55	-	-	-	0.1	0.1 M sodium phosphate buffer at pH 6.8	4
Pt	-0.06	5-10	99	-	-	-	0.08	0.1 M H_2SO_4	8
Rh	-0.8	-	5	-	-	95	0.08	isopropanol, water and acetic acid mixture	9
Ru	-0.8	-	25	-	-	75	0.08	isopropanol, water and acetic acid mixture	9

Table S2. Percentage composition of singe-atom catalysts calculated using XPS.

Sample	C1s (wt%)	N1s (wt%)	O1s (wt%)	Cu/Co 2p (wt%)
CuPc:MWCNT 1:20	94.39	1.94	2.02	1.65
CoPc:MWCNT 1:20	94.93	1.81	2.05	1.21

Table S3. the calculated adsorption energy of furfural on graphene-supported Cu/CoPc using RPBE-D3 and HSE06 functionals (in eV).

Surfaces	RPBE-D3	HSE06	Δ
CoPc	-0.48	-0.29	0.19
CuPc	-0.38	-0.21	0.17

Supplementary figures

XPS Spectra

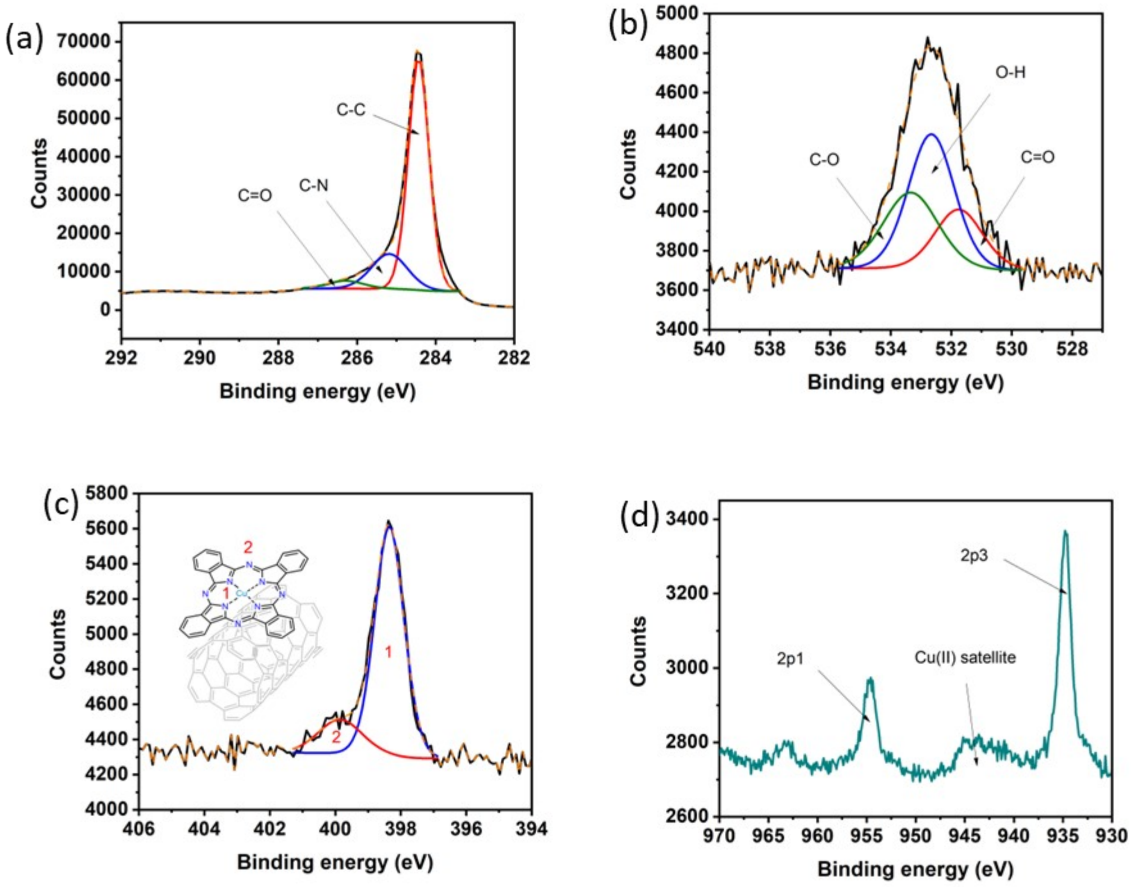

Figure S1. XPS spectra of CuPc adsorbed onto MWCNTs. (a) C1s, (b) O1s, (c) N1s and (d) Cu2p

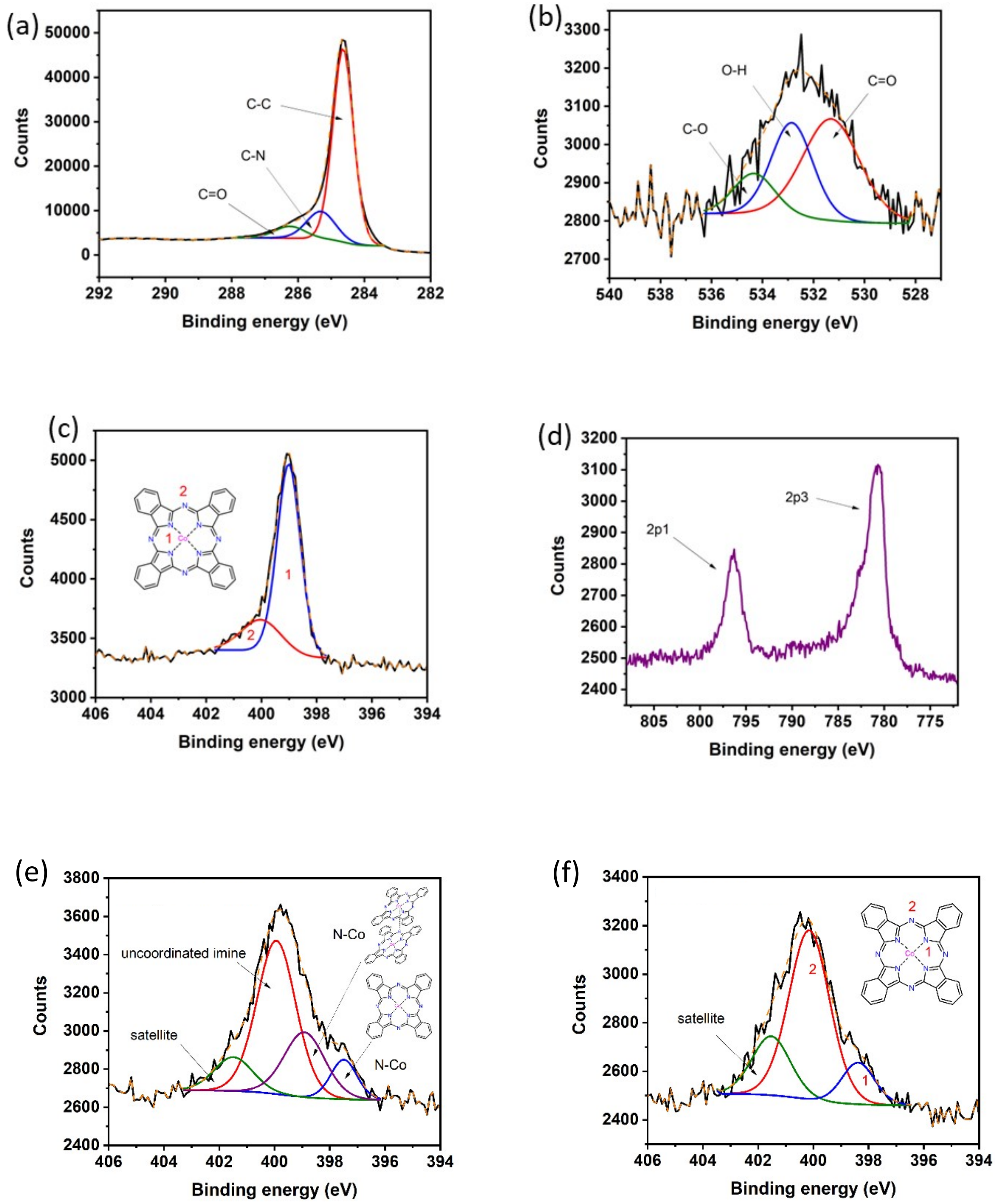

Fig S2. XPS spectra of CoPc adsorbed onto MWCNTs and carbon black. (a) C1s, (b) O1s, (c) N1s and (d) Co2p. (e) N1s XPS spectra of CoPc adsorbed onto carbon black before and (f) after electrochemistry.

The deconvolution of the N1s spectra for the CoPc on carbon black before electrochemistry displays 4 different binding energies corresponding to N coordinated to the main metal centre within the macrocycle, N coordinated to an adjacent phthalocyanine metal and the imine-bond N which is not involved in any non-covalent interaction. A satellite contribution can also be appreciated at higher binding energies.

After electrochemical testing, owing to the distortion in the crystal packing just 2 binding energies remain, these being the non-coordinated imine N and the N coordinated to the macrocycle metal.

For Co and Cu phthalocyanines supported on carbon nanotubes, the N1s spectra is substantially altered and the binding energies of the different nitrogen becomes harder to distinguish. This fact was previously observed by Basiuk and co-workers and was attributed to the strong bending distortion of macrocycle rings upon supramolecular interaction with the outer wall of carbon nanotubes.[10]

O1s spectra shows the chemical contributions of different functional groups in the surface of carbon paper and carbon nanotubes, mainly ketone (C=O) or hydroxyl (O-H) and also ether groups in the case of CNTs (C-O-C).[11]

HAADF-STEM

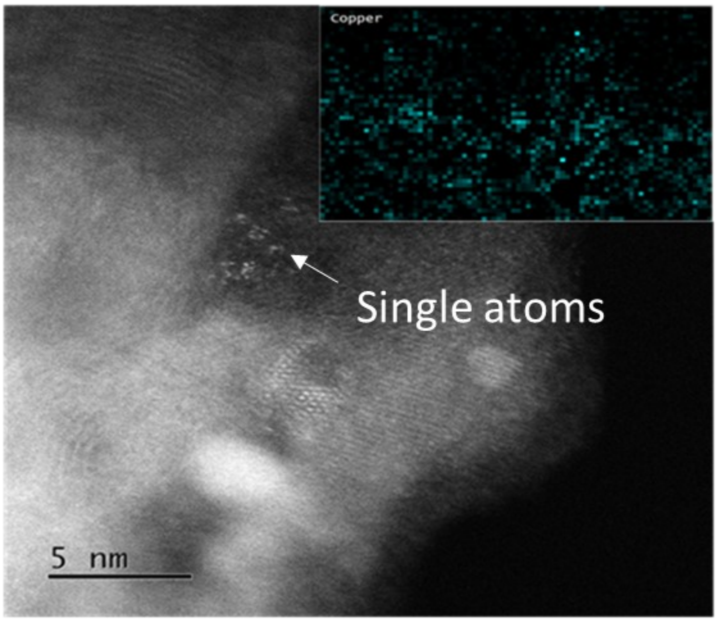

Fig S3. HAADF-STEM and energy dispersive x-ray image of CuPc adsorbed onto MWCNTs displaying single atoms sites present, along with minor clustering.

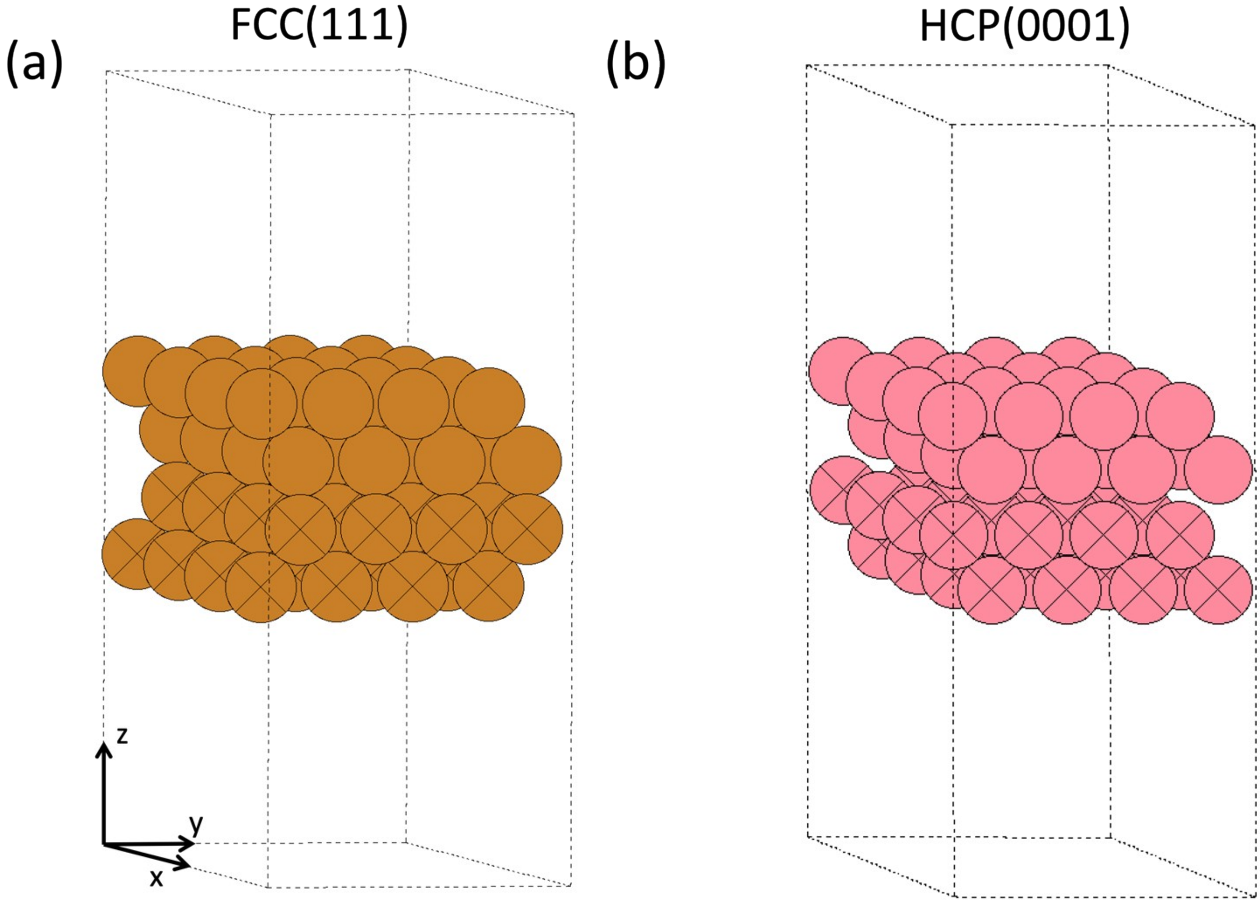

Fig. S4 Computational models for extended metal surfaces a) FCC(111): Au, Ag, Cu, Ni, Pb, Pt, Pd, and Rh, b) HCP(0001): Co and Ru.

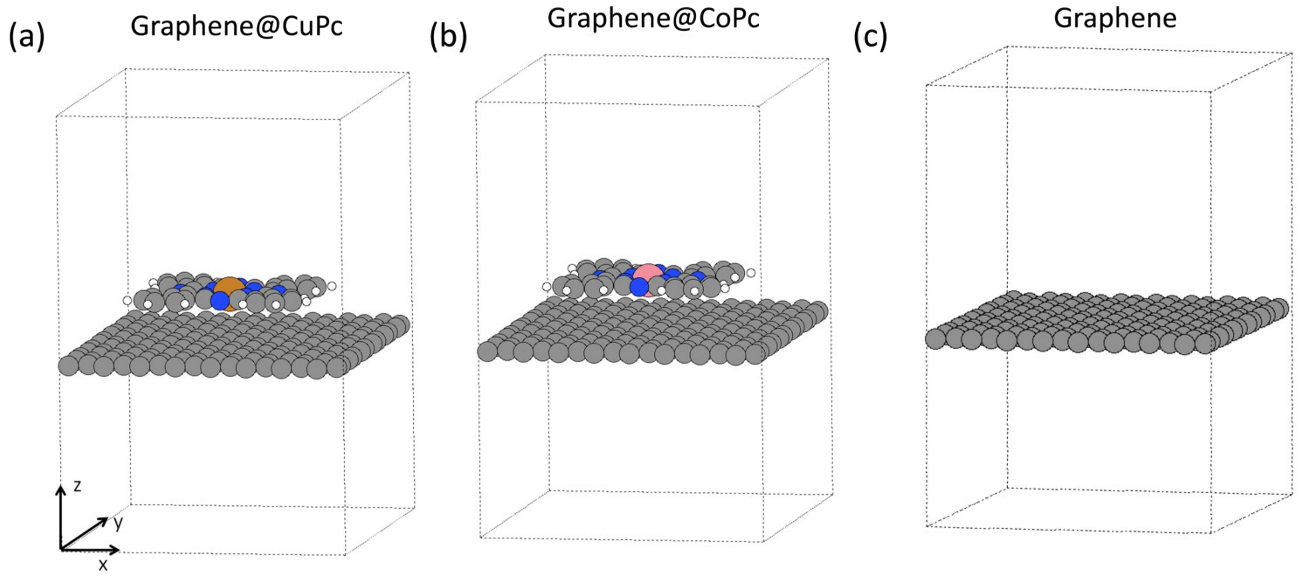

Fig. S5 Models for graphene and graphene-supported molecular single-atom catalysts in DFT calculations. a) graphene-supported CuPc, b) graphene-supported CoPc and c) single-layer graphene. Color codes: red-oxygen, white-hydrogen, grey-carbon, blue-nitrogen, brown-copper, pink-cobalt.

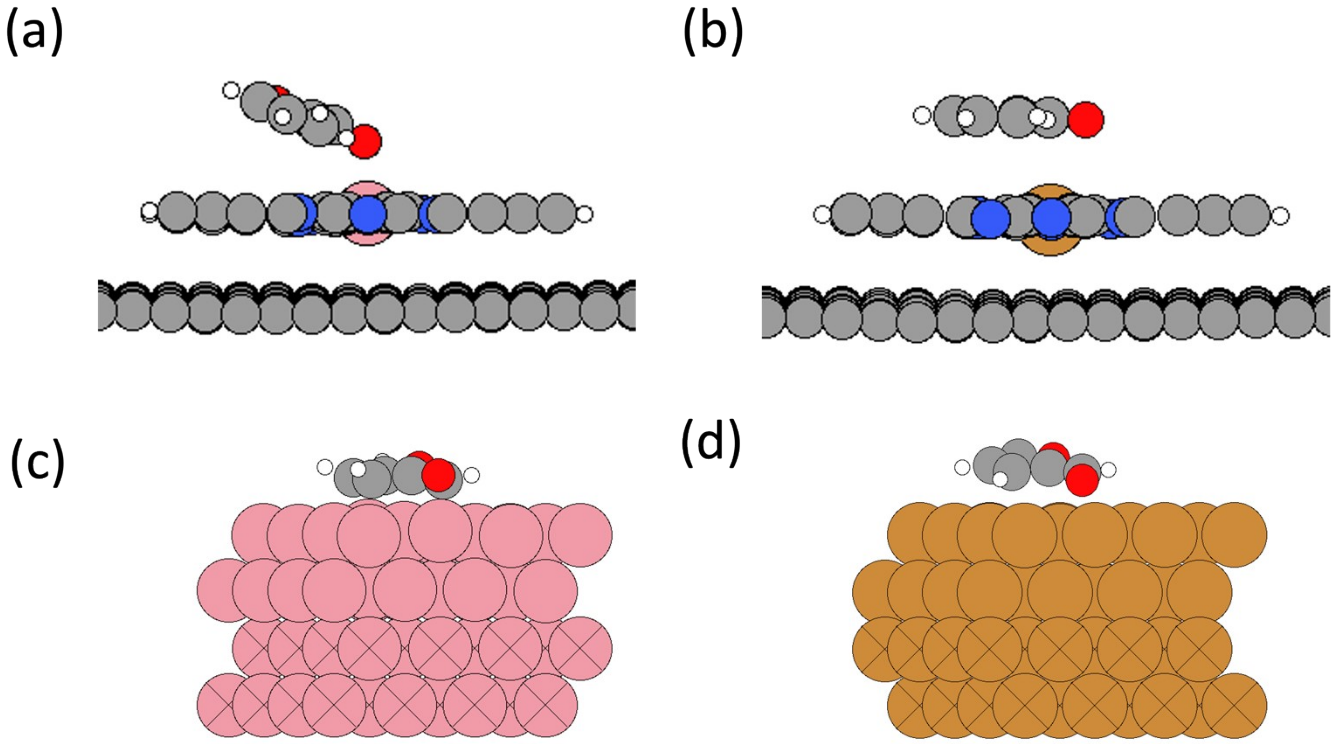

Fig S6. The optimized furfural adsorption on a) graphene-supported CoPc , b) graphene-supported CuPc , c) Co(0001) and d) Cu(111).

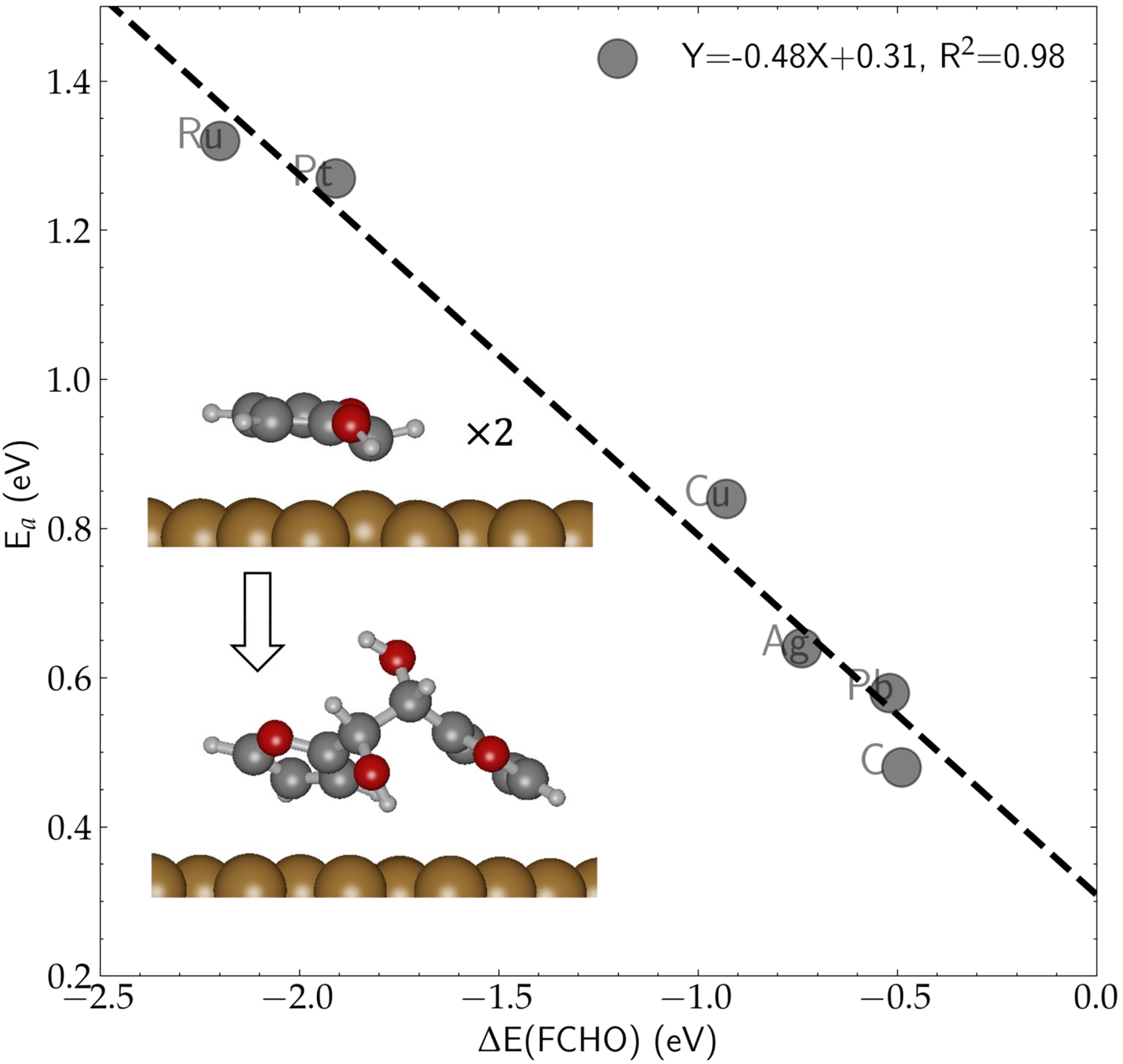

Fig. S7 The relationship between activation energies for coupling of two FCHOH* and the adsorption energies of furfural on extended metal surfaces. A showcase coupling process of FCHOH* to hydrofuroin is shown as the inset.

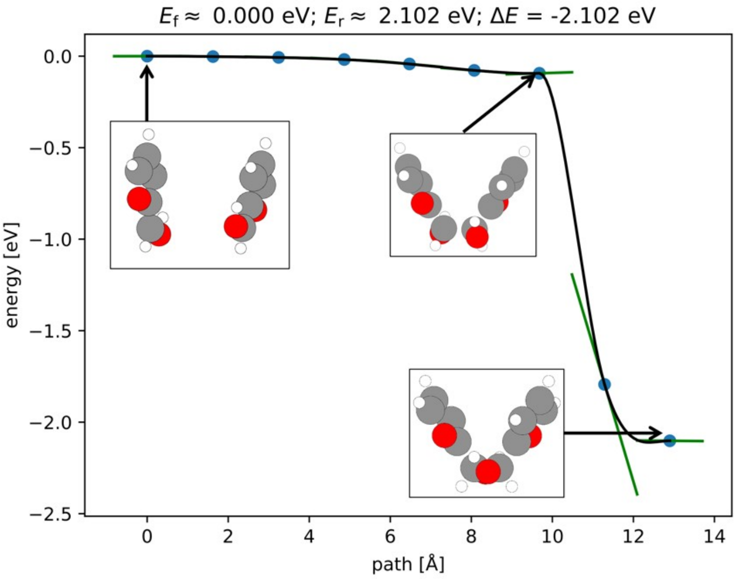

Fig. S8 The reaction trajectory of FCHOH· radical coupling in vacuum. The initial, transition and final states of the reaction are shown as insets in the figure. The very exothermic, barrierless and smooth reaction band suggests a facile FCHOH· coupling without surfaces.

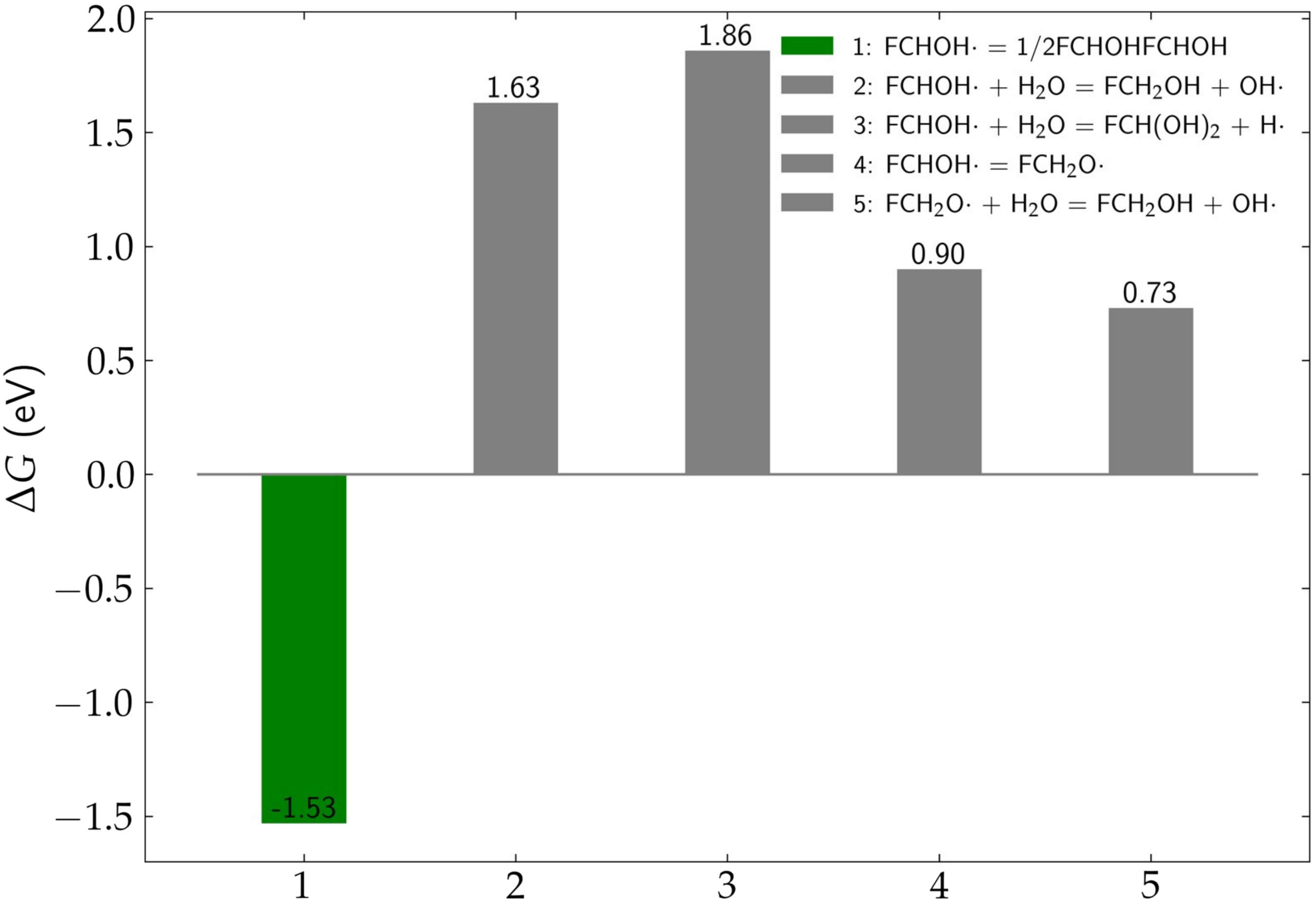

Fig. S9 The calculated Gibbs free energies of possible radical reactions for $FCHOH\cdot$.

NMR Spectra of Hydrofuroin

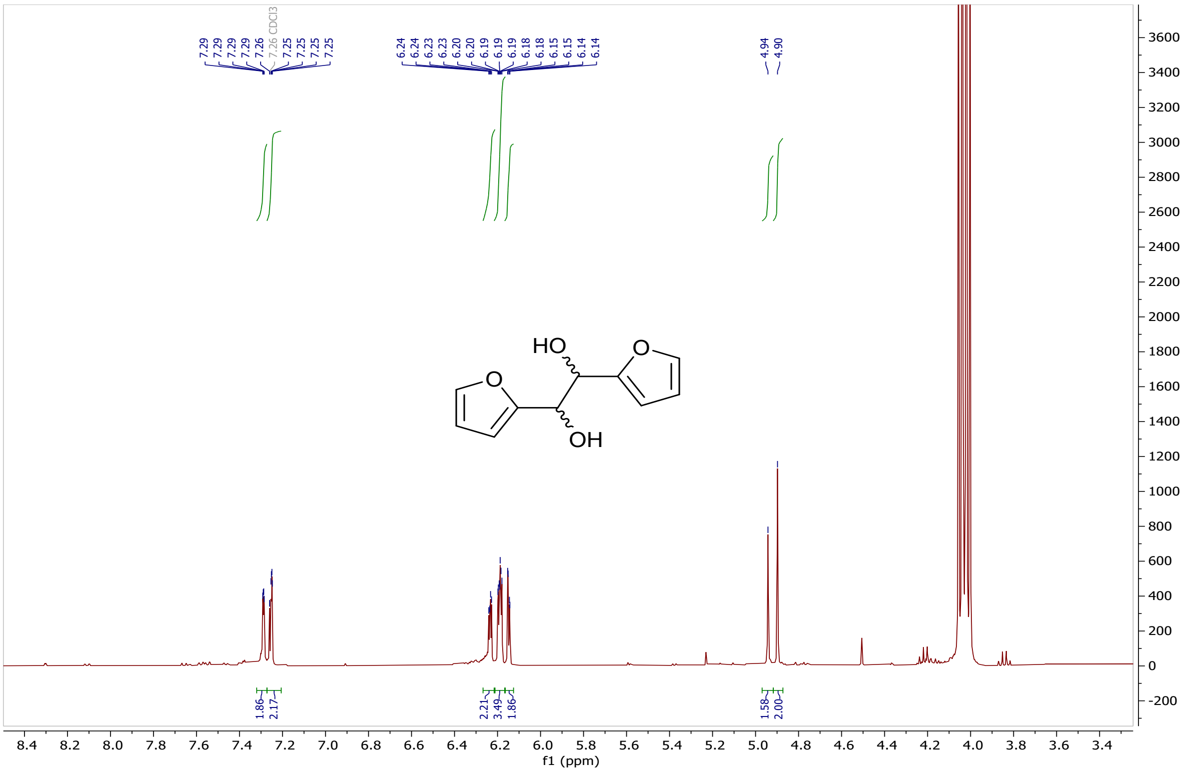

Fig S10. 400 MHz ^{1}H NMR spectra in $CDCl_3$ of hydrofuroin displaying both isomers. Large peak at ~4.0 ppm represents ethyl acetate solvent.

HPLC

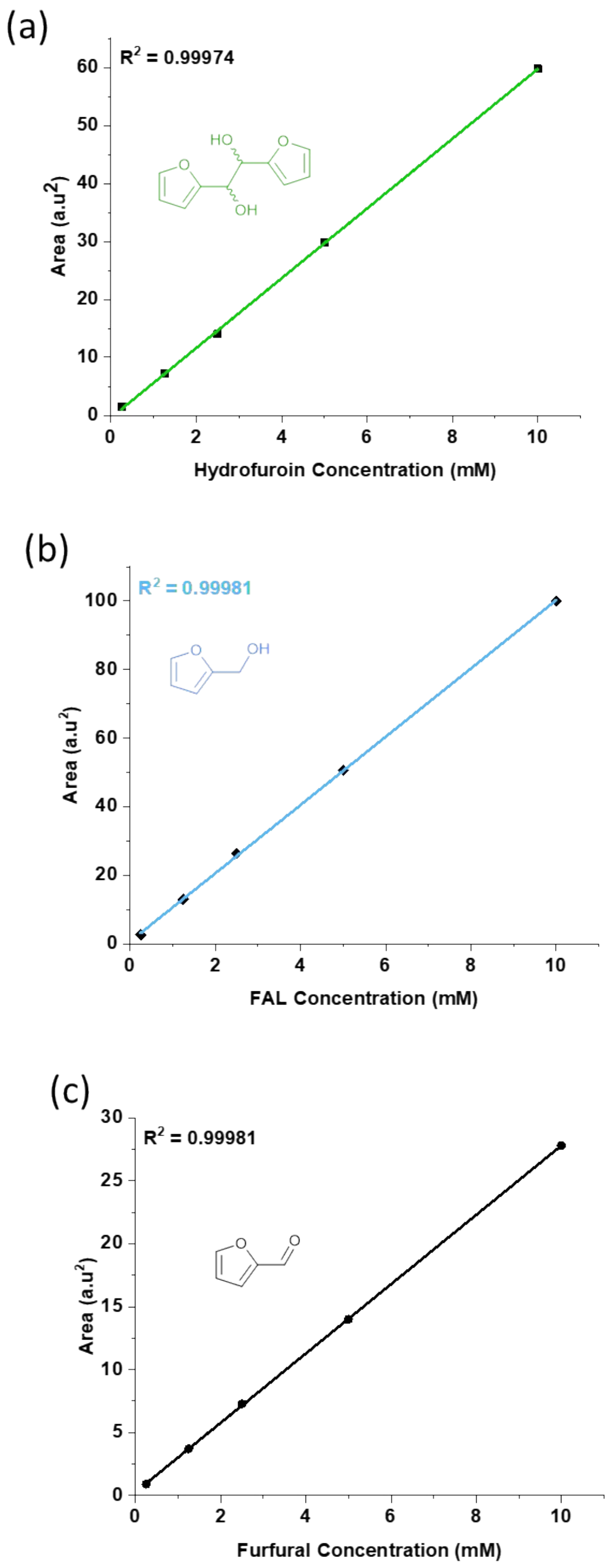

Fig S11. HPLC calibration curves of (a) hydrofuroin (b) FAL and (c) furfural at varying concentrations

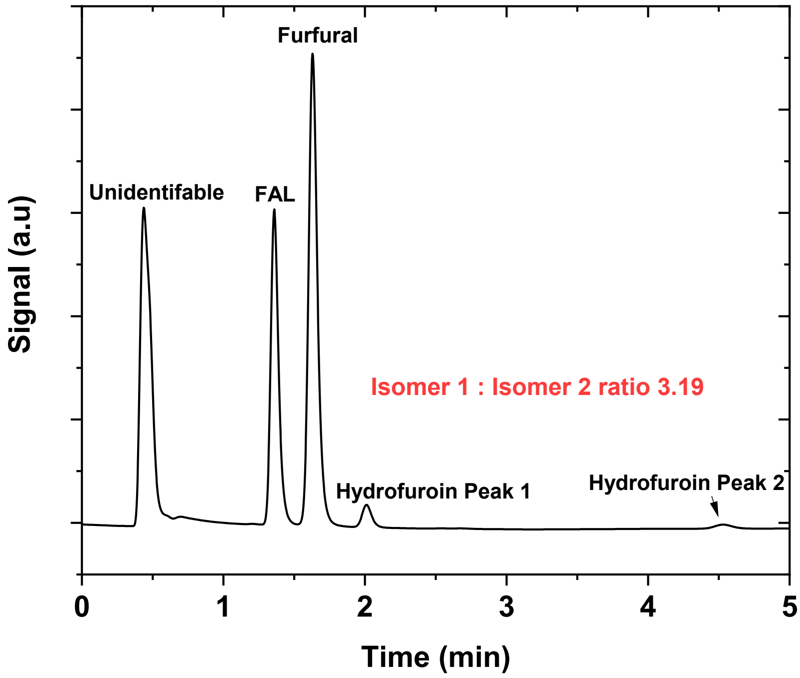

Fig S12. HPLC chromatogram of furfural reduction in pH 10 potassium bicarbonate buffer on a Cu electrode after 1 h at -0.50 V vs. RHE. We observe greater production of one isomer of hydrofuroin than the other indicating coupling could potentially be occurring on the surface opposed to in bulk solution.

ToF-SIMS

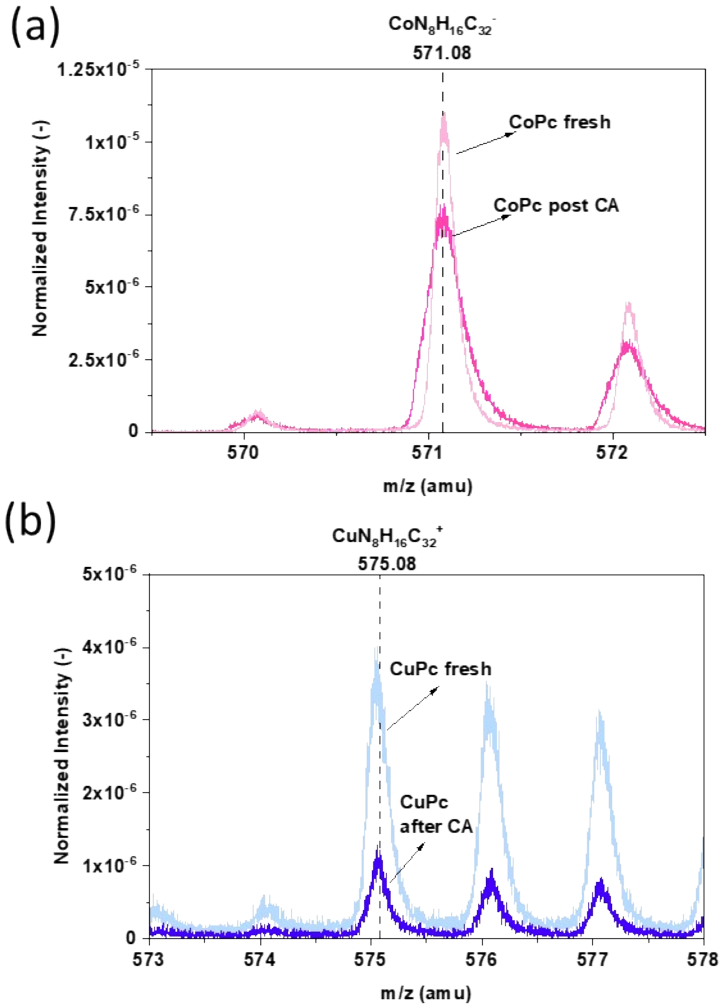

Fig S13. ToF-SIMS spectrum normalised to the total ion counts for fresh and post CA (a) CoPc and (b) CuPc with position of fragment in mass spectrum highlighted.

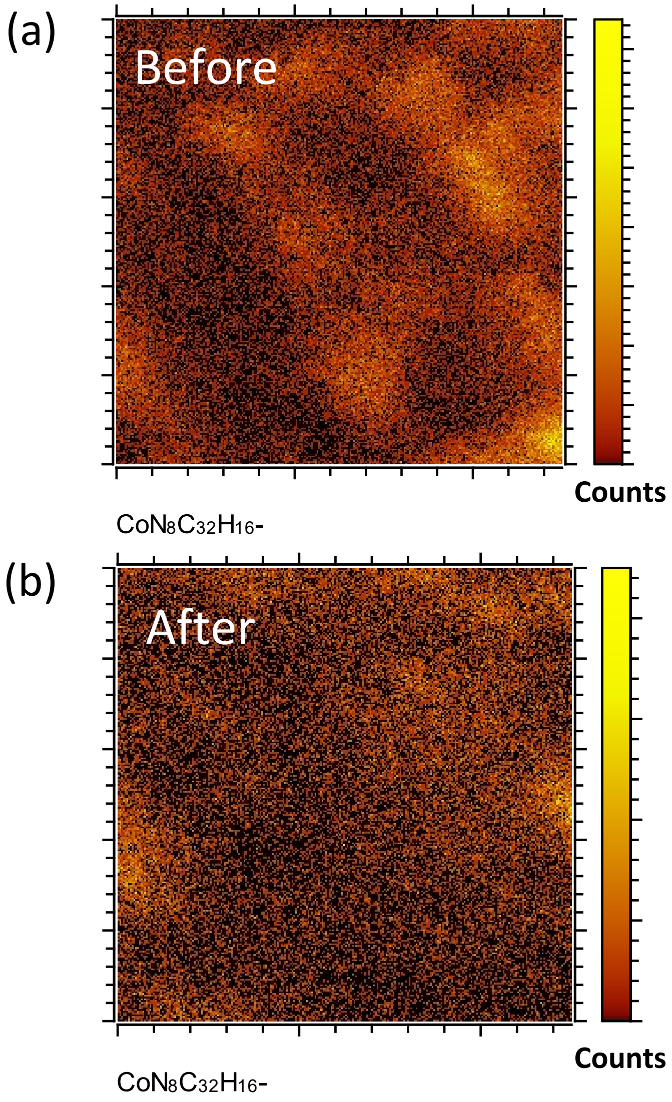

Fig. S14. ToF-SIMS negative imaging on (a) fresh and (b) post chromoamperometry CoPc.

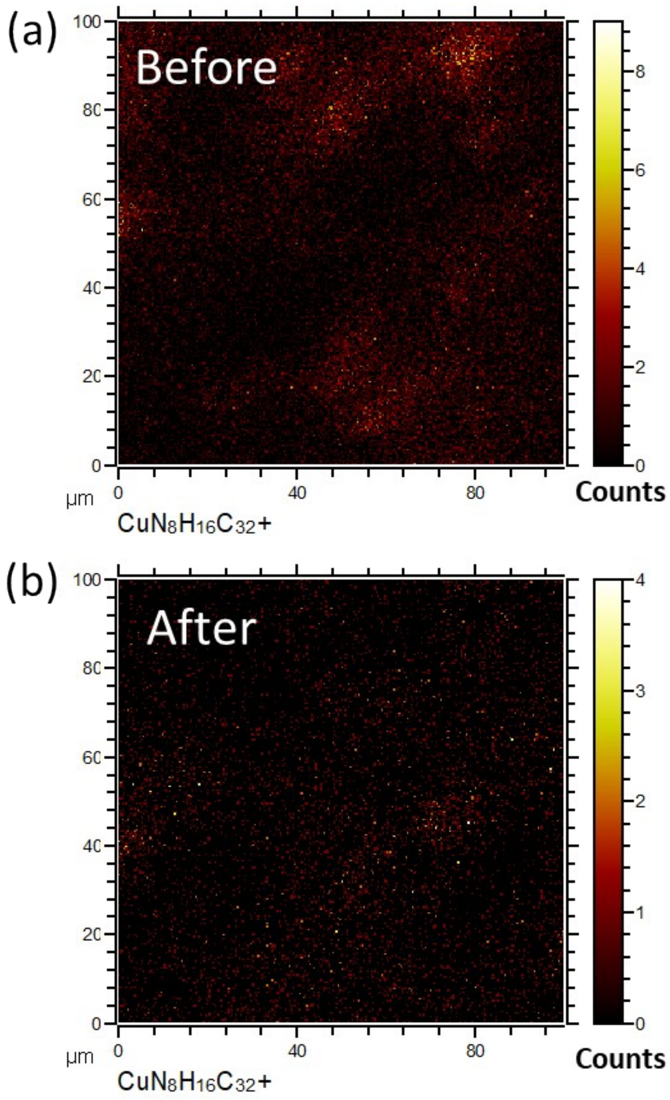

Fig. S15 ToF-SIMS positive imaging on (a) fresh and (b) post chromoamperometry CuPc.

Initial Concentration Experiments

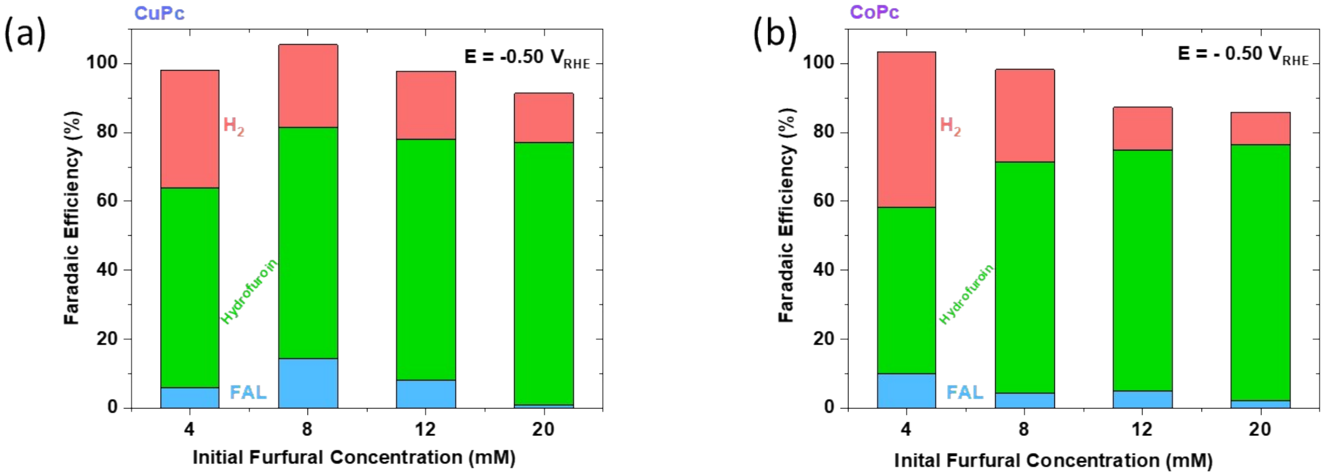

Fig S16. Faradaic efficiencies of detected products of furfural reduction at varying initial furfural concentrations on (a) CuPc and (b) CoPc. Experimental details: 0.1 M potassium bicarbonate buffer (pH 10), potential applied was -0.50 V vs. RHE for 1 h.

Varying Overpotential Experiments

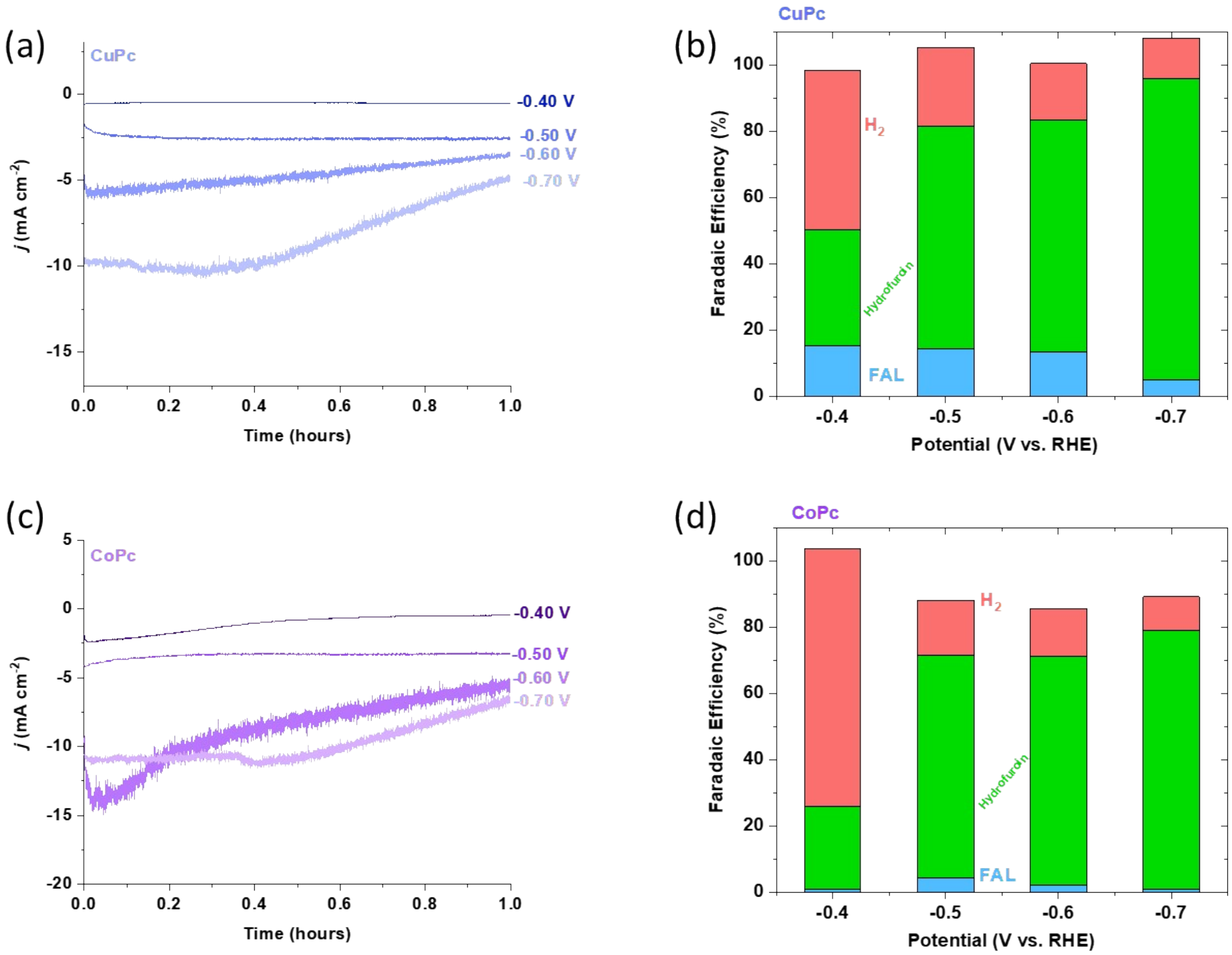

Fig S17. Varying overpotential studies of furfural reduction on single-atom catalysts. Constant potential measurements of (a) CuPc and (c) CoPc, with the corresponding Faradaic efficiencies of (b) CuPc and (d) CoPc. Experimental details: 0.1 M bicarbonate buffer (pH 10), 8 mM furfural, catalyst loading 0.1 mg cm^{-2}, for 1 h constant potential.

Extended Time Experiments

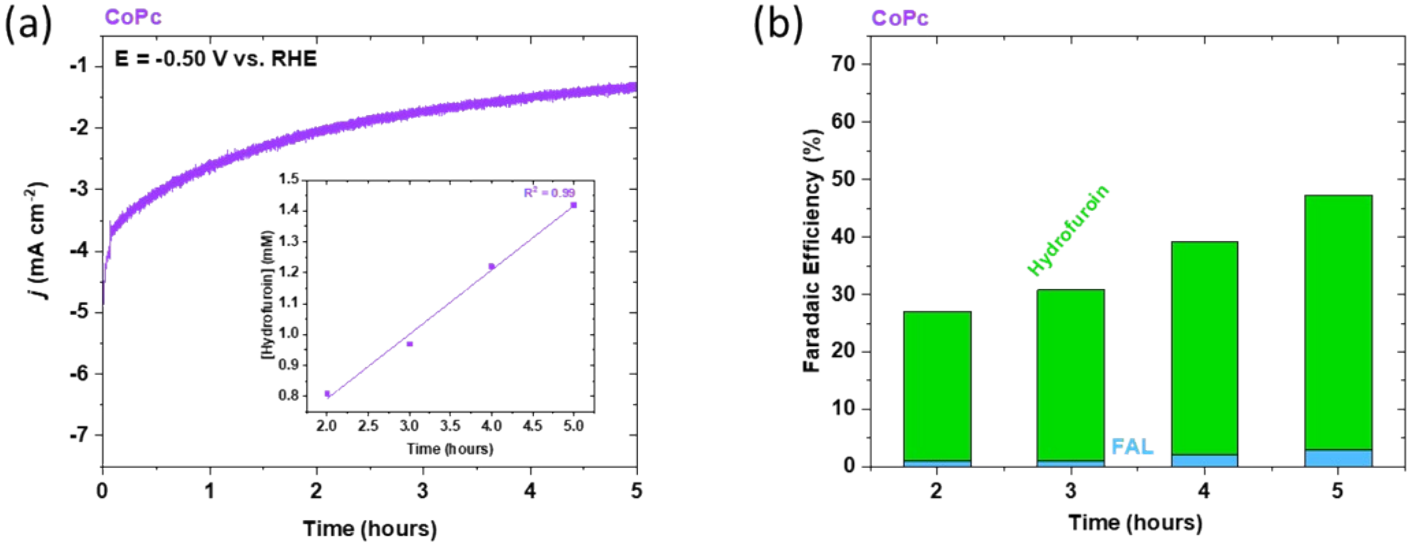

Fig S18. Extended constant potential measurements of CoPc. (a) 5 h constant potential of CoPc. Insert graph shows concentration of hydrofuroin production over 5 h. (b) corresponding Faradaic efficiencies of detected liquid products. Experimental details: 0.1 M bicarbonate buffer (pH 10), 8 mM furfural, catalyst loading 0.1 mg cm^{-2}, applied potential -0.50 V vs. RHE.

Onset Potential Comparisons

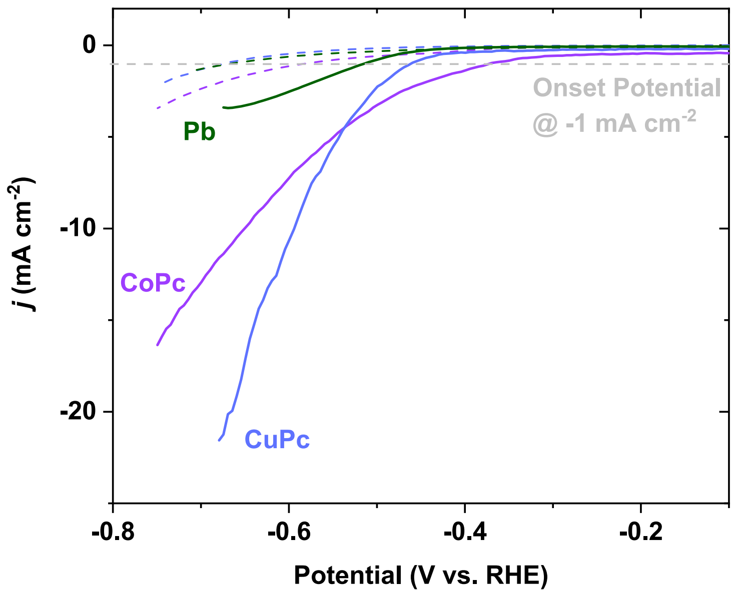

Fig S19. Linear sweep voltammograms of cathode materials before (dashed line) and after (solid line) the addition of 8 mM furfural. The onset potential is described as the potential at which a current density of -1 mA cm^{-2} is reached. Experimental details: 0.1 M bicarbonate buffer (pH 10), 8 mM furfural, Co/CuPc catalyst loading 0.1 mg cm^{-2}, scan rate 50 mV s^{-1}.

CoPc Reusability Experiments

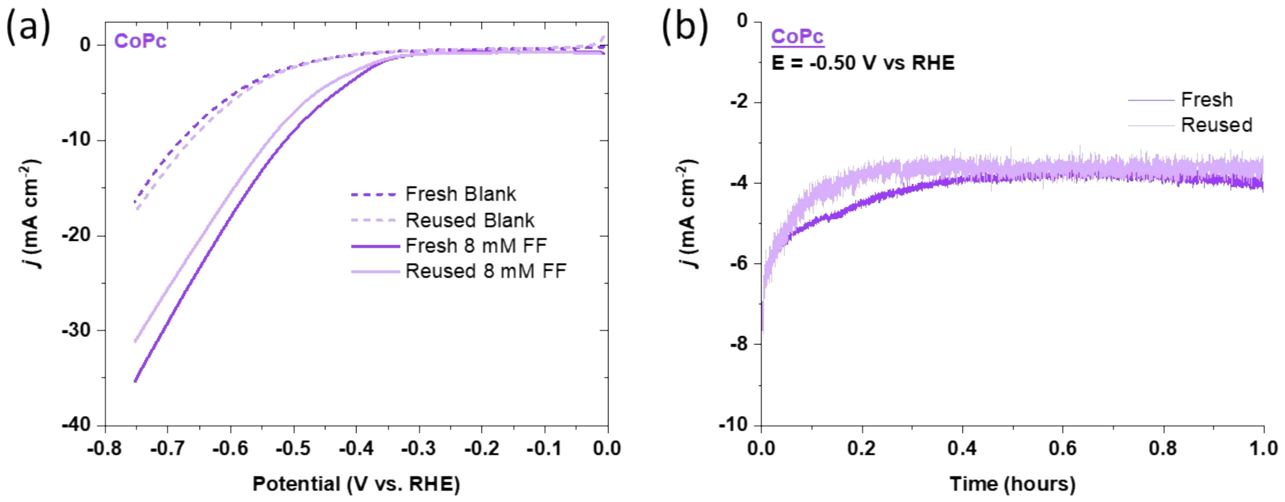

Fig S20. Investigation of the reusability of CoPc electrodes. (a) LSVs of fresh CoPc electrode before (dashed line) and after (solid line) the addition of 8 mM furfural (FF). (b) Constant potential measurements of fresh and reused electrode at -0.50 V vs RHE. Reaction conditions: 0.1 M potassium bicarbonate buffer (pH 10), 0.1 mg cm^{-2} catalyst loading, 8 mM furfural. The scan rate was 50 mV s^{-1}.

TOF Calculations

Turnover frequencies (TOFs) were calculated using the method of Mehmood et al.,[12] with the assumption that every metal atom (Co or Cu) is an active site on the surface of the electrode. The equations used to calculate TOFs are denoted below where A_r is the relative atomic mass, N_a is the Avogadro's constant ($6.023*10^{23}$), j_{HF} is the mass normalized current of hydrofuroin per gram of catalyst, and SD is the site density. Note that by using a conservative value (i.e., minimum) for site density, the resulting TOF reflects the upper end of the estimated spectrum of turnover frequencies.

At -0.50 V vs RHE, CoPc and CuPc have calculated TOFs of 0.40 ± 0.10 and 0.35 ± 0.01 hydrofuroin site^{-1} s^{-1} respectively, which can be used as comparison to other electrodes. Uncertainty values were obtained from two separate experiments.

$$Min\ Co\ Site\ Density\ \left[sites\ g^{-1}\right] = wt\%(Co)/A_r(Co)\left[g\ mol^{-1}\right] \times\ N_A\ \left[sites\ mol^{-1}\right]$$

$$j_{HF}\ \left[A\ g^{-1}\right] = e\ \left[C\ electron^{-1}\right] \times TOF\ \left[number\ of\ electrons/2\ site^{-1}s^{-1}\right] \times SD\ \left[site\ g^{-1}\right]$$

Supplementary references:

1 C. Reichardt, *Sugar Ser.*, 2000, **13**, 234–239.

2 J. K. Nørskov, J. Rossmeisl, A. Logadottir, L. Lindqvist, J. R. Kitchin, T. Bligaard and H. Jónsson, *J. Phys. Chem. B*, 2004, **108**, 17886–17892.

3 P. Nilges and U. Schröder, *Energy Environ. Sci.*, 2013, **6**, 2925.

4 J. T. Brosnahan, Z. Zhang, Z. Yin and S. Zhang, *Nanoscale*, 2021, **13**, 2312–2316.

5 R. S. Delima, M. D. Stankovic, B. P. Macleod, A. G. Fink, M. B. Rooney, A. Huang, R. P. Jansonius, D. J. Dvorak and C. P. Berlinguette, *Energy Environ. Sci.*, 2022, **15**, 215–224.

6 X. H. Chadderdon, D. J. Chadderdon, J. E. Matthiesen, Y. Qiu, J. M. Carraher, J. Tessonnier and W. Li, *J. Am. Chem. Soc.*, 2017, **139**, 14120–14128.

7 P. Zhou, Y. Chen, P. Luan, X. Zhang, Z. Yuan, S. X. Guo, Q. Gu, B. Johannessen, M. Mollah, A. L. Chaffee, D. R. Turner and J. Zhang, *Green Chem.*, 2021, **23**, 3028–3038.

8 B. Zhao, M. Chen, Q. Guo and Y. Fu, *Electrochim. Acta*, 2014, **135**, 139–146.

9 J. A. Lopez-Ruiz, E. Andrews, S. A. Akhade, M. S. Lee, K. Koh, U. Sanyal, S. F. Yuk, A. J. Karkamkar, M. A. Derewinski, J. Holladay, V. A. Glezakou, R. Rousseau, O. Y. Gutiérrez and J. D. Holladay, *ACS Catal.*, 2019, **9**, 9964–9972.

10 E. V. Basiuk, L. Huerta and V. A. Basiuk, *Appl. Surf. Sci.*, 2019, **470**, 622–630.

11 S. Kundu, Y. Wang, W. Xia and M. Muhler, *J. Phys. Chem. C*, 2008, **112**, 16869–16878.

12 A. Mehmood, M. Gong, F. Jaouen, A. Roy, A. Zitolo, A. Khan, M. T. Sougrati, M. Primbs, A. M. Bonastre, D. Fongalland, G. Drazic, P. Strasser and A. Kucernak, *Nat. Catal.*, 2022, **5**, 311–323.